Supplementary Information for
Reactive Plasma Cleaning and Restoration of Transition Metal Dichalcogenide Monolayers

Daniil Marinov,[1] Jean-François de Marneffe[a],[1] Quentin Smets,[1] Goutham Arutchelvan,[1] Kristof M. Bal,[2] Ekaterina Voronina,[3] Tatyana Rakhimova,[3] Yuri Mankelevich,[3] Salim El Kazzi,[1] Ankit Nalin Mehta,[1,4] Pieter-Jan Wyndaele,[1,5] Markus Hartmut Heyne,[1,5,2] Jianran Zhang,[1] Patrick C. With,[6,1] Sreetama Banerjee,[1] Erik C. Neyts,[2] Inge Asselberghs,[1] Dennis Lin,[1] and Stefan De Gendt[1,5]

[1]*imec v.z.w., Kapeldreef 75, B-3001 Leuven, Belgium*
[2]*Department of Chemistry, University of Antwerp,*
Universiteitsplein 1, 2610 Antwerp, Belgium
[3]*1 Skobeltsyn Institute of Nuclear Physics, Moscow State University,*
GSP-1 Leninskie Gori 1, Moscow 119234, Russia
[4]*Department of Physics and Astronomy, KU Leuven,*
Celestijnenlaan 200F, 3001 Leuven, Belgium
[5]*Department of Chemistry, KU Leuven,*
Celestijnenlaan 200F, 3001 Leuven, Belgium
[6]*Leibniz Institute of Surface Engineering (IOM),*
Permoserstrasse 15, D-04318 Leipzig, Germany

---

[a] Corresponding author: marneffe@imec.be.

In order to investigate the mechanisms of material modification under remote H_2 plasma exposure we carried out DFT simulations of H interaction with single layer WS_2. Hydrogen atoms can adsorb and diffuse on the WS_2 surface and eventually create S-vacancies via H_2S release. Here we discuss the most relevant surface processes identified by ab-initio simulations.

I.   SUPPLEMENTARY METHODS

Two DFT models of atomic H reactivity on WS_2 were compared in this study. Both models were based on the Perdew–Burke–Ernzerhof (PBE) [1] exchange-correlation functional within the generalized gradient approximation (GGA), to which the first model applied the Hubbard correction for strongly correlated systems (GGA+U approach [2]) within a plane wave basis set (DFT+U/PW model), whereas the second model employed the uncorrected PBE functional within a local atomic orbital basis (DFT/AO model). The nudged elastic band (NEB) method [3] was applied to calculate energy barriers for the migration and desorption of species in most cases. The DFT+U/PW simulations were carried out with the Vienna Ab Initio Simulation Package (VASP)4 on "Lomonosov-2" supercomputer of Lomonosov Moscow State University [4, 5]. Projector-augmented wave (PAW) [6] pseudopotentials were used to describe the interaction between the core and valence electrons. The model of the WS_2 monolayer consisted of 4 x 4 unit cells. Periodic boundary conditions were applied, and in order to avoid interaction between periodic images, the vacuum separation along the Z direction was set to be 20 Å. A plane wave basis set with 500 eV energy cutoff was used, and the Brillouin zone was sampled by 6 x 6 x 1 k-points in accordance with the Monkhorst-Pack scheme. DFT/AO calculations were carried out using the CP2K package in the mixed Gaussian & plane wave (GPW) formalism [7]. The valence Kohn–Sham orbitals were expanded in a doubly polarized triple zeta basis set (m-TZV2P [8]) in combination with GTH-type pseudopotentials for the core electrons [9]. The density was represented with an auxiliary plane wave basis defined by a cutoff of 800 Ry. A larger periodic WS_2 monolayer model of 6 x 6 unit cells was used, and periodicity along the Z direction was removed through application of the Martyna–Tuckerman Poisson solver [10].

The calculation approach used for the [WS_2+OCS] system is identical as the one used for the [WS_2+H]. Since both DFT+U/PW and DFT/AO models gave similar results on the

[WS$_2$+H], only the DFT+U/PW was used for the [WS$_2$+OCS] calculations.

II. SUPPLEMENTARY DISCUSSION

A. DFT Simulation of H atoms interactions with WS$_2$

The Supplementary Table I shows the most relevant reactions that are described in this paragraph, together with associated activation energies calculated by the DFT+U/PW and DFT/AO models (in the following discussion, for the sake of clarity, only energies calculated by the DFT+U/PW model are mentioned). Simulations predict that H atoms adsorb preferentially on surface S atoms forming a surface SH$_{surf}$ group (reaction (1) in Table I). Several possible adsorption sites were identified, but the so-called 'tilted' position, where the adsorbed H atom is located near an S atom at the angle of 50° to the monolayer plane, is energetically preferential (see Figure 1(a)). The adsorption energy for this site is 0.53 eV. Under the remote hydrogen plasma conditions, adsorption of H atoms from the gas phase and thermal desorption (reaction (2) in Table I) control the coverage of SH$_{surf}$ groups on the surface. An adsorbed H atom can change its orientation or migrate along the WS$_2$ surface (reaction (3) in Table I). The calculated activation barriers for the rotation of H around the S atom above one of the adjacent W–S bonds and for migration between two S atoms within the same unit cell are equal to 0.29 and 0.34 eV, respectively, i.e. well below the H desorption barrier.

DFT simulations predict clustering of H atoms as the result of their migration along the surface. When an H atom migrates from an existing SH$_{surf}$ group to another SH$_{surf}$ group, a surface H$_2$S complex can be formed (reaction (4) in the Supplementary Table I). An identical surface H$_2$S complex is formed if an impinging H atom meets an SH$_{surf}$ group (reaction (5) in the Supplementary Table I). The Supplementary Figure 1 illustrates the energy diagram of this process. The H$_2$S$_{surf}$ complex can be released (with an activation energy of E$_a$ = 0.66 eV) from the surface as a volatile H$_2$S molecule leaving a sulphur vacancy behind (reaction (8)). A competing process occurs when two H atoms meet, forming a gas-phase H$_2$(g) that extracts hydrogen from the surface without causing sulphur depletion (reaction (9)). This process has, however, a lower barrier than the clustering of adjacent H atoms into the H$_2$S$_{surf}$ complex. Likewise, the H$_2$S release, reaction (8), has a lower barrier

TABLE I: Surface reactions relevant to WS_2 damage by atomic hydrogen and corresponding activation energies. LH = Langmuir-Hinshelwood type of reaction; ER = Eley-Rideal type of reaction. Compared DFT models: +U/PW and AO (see body text). Activation energies are expressed in eV.

Process	Reaction detail	+U/PW	AO
		eV	eV
H adsorption	$SH_{surf} + H(g) \rightarrow SH_{surf}$ (1)	0	0
H desorption	$SH_{surf} \rightarrow S_{surf} + H(g)$ (2)	0.53	0.40
H migration	$SH_{surf} + S_{surf} \rightarrow S_{surf} + SH_{surf}$ (3)	0.34	0.30
H_2S_{surf} formation-LH	$SH_{surf} + SH_{surf} \rightarrow S_{surf} + H_2S_{surf}$ (4)	0.39	0.28
H_2S_{surf} formation-ER	$H(g) + HS_{surf} \rightarrow H_2S_{surf}$ (5)	0	0
Reaction (4) reversed	$H_2S_{surf} + S_{surf} \rightarrow SH_{surf} + SH_{surf}$ (6)	0.70	0.74
H_2S release-ER	$H(g) + SH_{surf} \rightarrow S_{vacancy} + H_2S(g)$ (7)	< 0.66	–
H_2S release	$H_2S_{surf} \rightarrow S_{vacancy} + H_2S(g)$ (8)	0.66	0.39
H_2 formation-LH	$SH_{surf} + SH_{surf} \rightarrow S_{surf} + H_2(g)$ (9)	0.51	0.54
H_2 formation-ER	$H(g) + SH_{surf} \rightarrow S_{surf} + H_2(g)$ (10)	0	0
H adsorption at $S_{vacancy}$	$S_{vacancy} + H(g) \rightarrow S_{vacancy}H_{subsurf}$ (11)	0	0

than the break-up process (6) of the H_2S_{surf} complex. Both DFT models therefore agree that, once adsorbed H atoms are present, sulphur depletion is a kinetically and thermodynamically favored phenomenon, with the final desorption step (8) being exothermic by 0.66 eV (DFT+U/PW) or 0.39 eV (DFT/AO).

It should be noted that there is a more probable process of H_2S release from the surface, namely, reaction (7) of SH_{surf} interaction with an incident H atom from the gas phase (H(g) atom). This process can proceed via singlet and triplet intermediate states and the details of these pathways will be described elsewhere. In addition to the above-mentioned Langmuir-Hinshelwood (LH) reactions, H_2S_{surf} and $H_2(g)$ can be formed in a direct Eley-Rideal (ER) impact between incident H(g) atoms and SH_{surf} groups (reactions (5) and (10), respectively). The H atom adsorption at an S-vacancy (reaction (11)) results in a sub-surface H atom with a binding energy much larger than the $S_{surf}H$ binding energy. These predictions were confirmed by dynamic DFT simulations of interactions of 0.1 – 1.0

eV H atoms with the MoS_2 and WS_2 monolayers (the results on MoS_2, obtained by dynamic simulations, have been reported previously [11]).
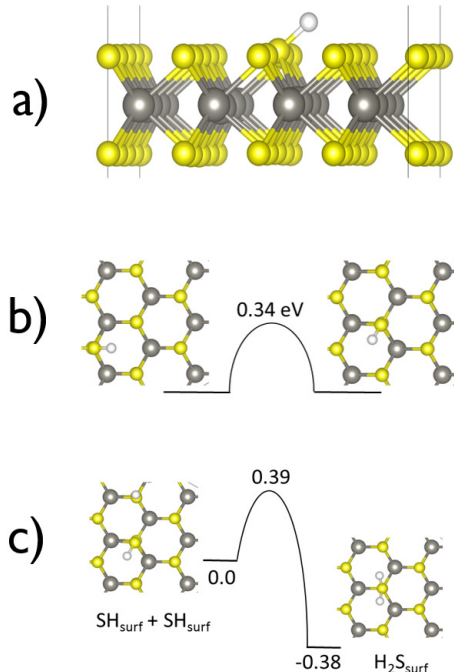
Supplementary Fig. 1. Schematic illustrations of DFT-calculated mechanisms of H interaction with WS_2: a) H adsorption in tilted position; b) energy diagram for surface diffusion; c) energy diagram for surface H_2S group formation.

As one can infer from the Supplementary Table I, the rate of H_2S_{surf} production and hence the rate at which sulphur vacancies are formed is proportional to the coverage of surface SH_{surf} groups. It is therefore crucial that this coverage remains low. The main effect of WS_2 surface temperature on the H_2S elimination rate could be related with the thermal desorption of H atoms from WS_2 surface (i.e. from SH groups with S-H binding energy E_a =0.53 eV, Supplementary Table I). The rate coefficient $\nu[s^{-1}]$ of H thermal desorption can be estimated as $\nu(T) = 10^{13}\exp(-E_a/k_B T)$[12]. The variation of T from 393 to 573 K results in a two order of magnitude increase of the desorption frequency ($\nu(393$ K$)$ = 1.6×10^6 s^{-1} vs $\nu(573$ K$) = 2.2 \times 10^8$ s^{-1}) and respective decrease of the SH_{surf} coverage. Likewise, high temperatures will increase the relative importance of LH desorption of H_2 (reaction (9)) versus clustering. Such a dramatic decrease of the SH_{surf} coverage (and hence the rate of $H_2S(g)$ and $S_{vacancy}$ formation) explains the unexpected reduction of the WS_2

damage at elevated surface temperatures observed in the experiments. Additional DFT simulations (not presented here) showed that H reactivity on MoS_2 monolayers is similar to the case of H - WS_2 system. It is therefore expected that remote hydrogen plasma will be efficient for cleaning MoS_2 and other TMDs.

B.   S vacancy healing with OCS molecules

An OCS molecule is a logical candidate for healing S vacancies on WS_2 surfaces since it can dissociate into CO and S fragments. The dissociation energy of the OCS molecule is of 3.1 eV [13, 14], but the calculated energy of healing S vacancy on the WS_2 layer by an S atom is $\sim$ 6.1 eV, so the overall process is exothermic. As our DFT simulation showed the OCS molecule can be absorbed on the WS_2 surface above the vacancy with the absorption energy of $\sim$ 0.5 eV (Supplementary Figure 2(a)). In this configuration, the molecule is inclined slightly with respect to the vertical axis, while S atom is directed towards the vacancy and located at the distance of 2.6 Å from the plane going through the upper sulfur layer. At the closer approaching to the surface, the OCS molecule could dissociate on CO and S fragments (Supplementary Figure 2(b)) which leads to the S vacancy healing and the formation of a volatile CO molecule (Supplementary Figure 2(c)). However, the activation barrier of this process is too high ($\sim$ 1.1 eV) so this dissociation pathway is not realistic under experimental conditions. There is a possibility of the OCS molecule absorption above the S vacancy in the position with an O atom directed to the surface with the absorption energy of $\sim$ 0.3 eV and distance of 2.4 Å, but the dissociation of the molecule into CS and O fragments is endothermic in this case, so the vacancy filling by an O atom can be hardly realized. The dissociative adsorption of OCS molecule at $S_{vacancy}H_{subsurf}$ site with the CO molecule release is also complicated due to the high barrier $>$ 1 eV.

A more realistic mechanism of S vacancy healing could be related to the OCS reactions with H atoms adsorbed on the WS_2 monolayer and/or reactor wall. In this case, the dissociation of the OCS molecule could proceed via the following two-step process shown in Supplementary Figure 3:

$$H_{surf} + OCS_{gas} \rightarrow OCSH_{gas} \tag{12}$$

$$S_{vacancy} + OCSH_{gas} \rightarrow SH_{surf} + CO_{gas} \tag{13}$$
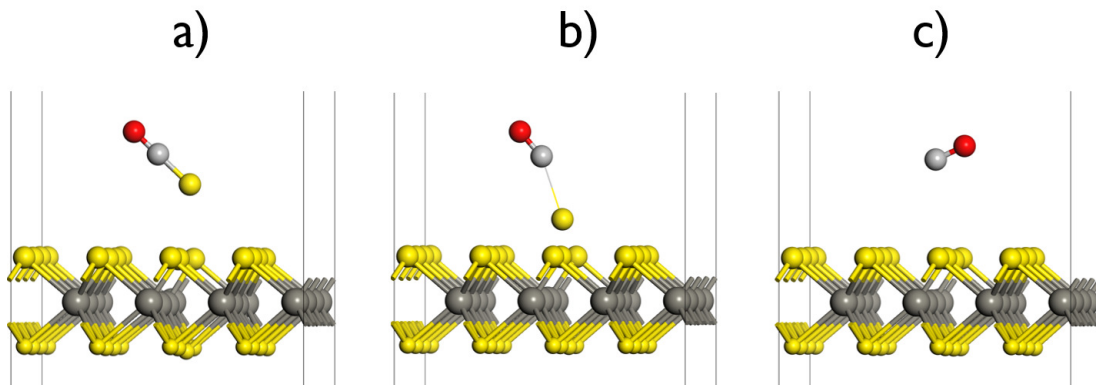
Supplementary Fig. 2. Preferential configuration of the OCS molecule absorption on the WS$_2$ monolayer with an S vacancy (a), the intermediate (b) and final (c) states of the process of OCS molecule near the S vacancy.

The Supplementary Figure 3(a-c) shows the pathways of reaction (12) for the abstraction of an H atom from the hydrogenated WS$_2$ surface with formation of the OCSH molecule, while the Supplementary Figure 3(d-f)) corresponds to reaction (13) of the OCSH dissociation on a S vacancy resulting in the release of a volatile CO molecule. DFT modeling shows that the first process is exothermic (the reaction energy, ΔE, is $\sim$ -0.1 eV) and has an activation barrier of 0.2–0.3 eV. During the reaction (12), an H addatom attaches to the S atom resulting in bending of the OCS molecule and converting of the double C=S bond into a single C–S bond in the produced O=C–S–H molecule. Therefore, the weakened C–S bond promotes dissociation of OCSH radicals in interactions with S-vacancies on the surface.

Reaction (13) is exothermic, too, with $\Delta E = -1.7$ eV, and it leads to breaking of the single C–S bond and adsorption of a SH radical on the S-vacancy. It proceeds only at favorite orientation of the OCSH molecule, namely, with the S atom directed to the surface. This orientation is not energetically preferable, and the lowest energy of the system corresponds to the configuration shown in the Supplementary Figure 3(c). However, the overall barrier of reaction (13) is only 0.2–0.3 eV with respect to the energy of this configuration, so the healing reaction could proceed in the experimental conditions under study. We can conclude that S-vacancy healing with thermal OCS molecules can be realized via two-step process: formation (by H abstraction) of the OCSH molecule and further dissociation (OC–SH bond
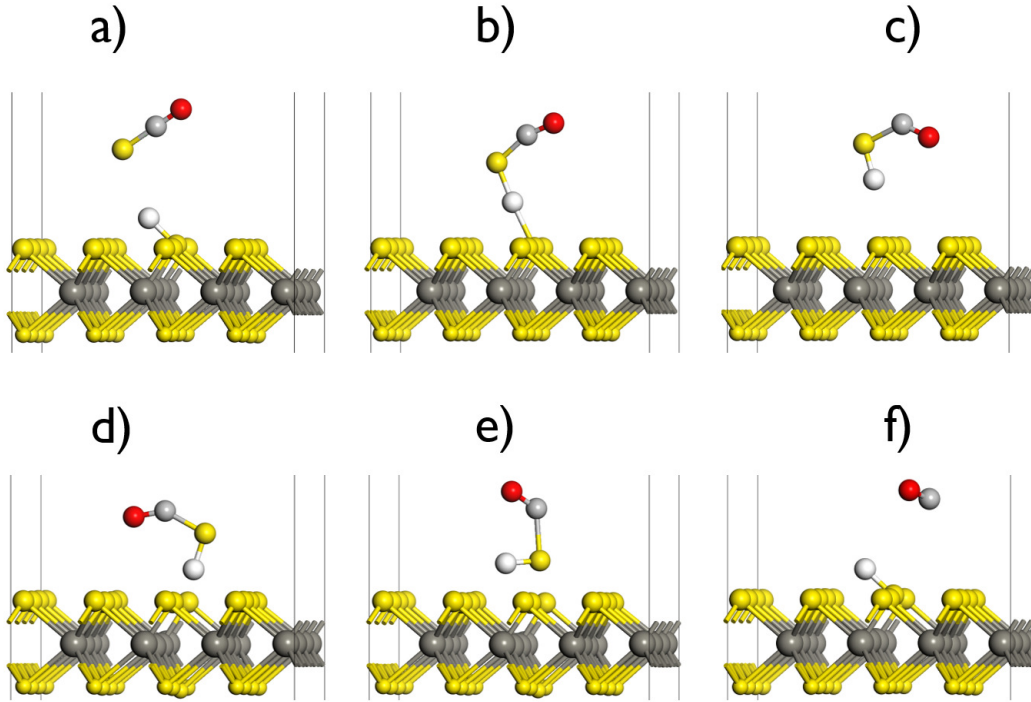
Supplementary Fig. 3. Pathways for the OCS molecule dissociation on the hydrogenated WS$_2$ surface: (a–c): reaction (12); (d–f): reaction (13).

breaking) on the S vacancy.

[1] Perdew, J. P., Burke, K. & Ernzerhof, M. Generalized gradient approximation made simple. *Phys. Rev. Lett.* **77**, 3865–3868 (1996). URL https://link.aps.org/doi/10.1103/PhysRevLett.77.3865.

[2] Dudarev, S. L., Botton, G. A., Savrasov, S. Y., Humphreys, C. J. & Sutton, A. P. Electron-energy-loss spectra and the structural stability of nickel oxide: An lsda+u study. *Phys. Rev. B* **57**, 1505–1509 (1998). URL https://link.aps.org/doi/10.1103/PhysRevB.57.1505.

[3] Mills, G., Jónsson, H. & Schenter, G. K. Reversible work transition state theory: Application to dissociative adsorption of hydrogen. *Surface Science* **324**, 305 – 337 (1995). URL http://www.sciencedirect.com/science/article/pii/0039602894007314.

[4] Kresse, G. & Furthmüller, J. Efficient iterative schemes for *ab initio* total-energy calculations using a plane-wave basis set. *Phys. Rev. B* **54**, 11169–11186 (1996). URL https://link.aps.

org/doi/10.1103/PhysRevB.54.11169.

[5] Voevodin, V. *et al.* Supercomputer lomonosov-2: Large scale, deep monitoring and fine analytics for the user community. *Supercomputing Frontiers and Innovations* **6** (2019). URL https://superfri.org/superfri/article/view/278.

[6] Kresse, G. & Joubert, D. From ultrasoft pseudopotentials to the projector augmented-wave method. *Phys. Rev. B* **59**, 1758–1775 (1999). URL https://link.aps.org/doi/10.1103/PhysRevB.59.1758.

[7] Hutter, J., Iannuzzi, M., Schiffmann, F. & VandeVondele, J. CP2K: Atomistic simulations of condensed matter systems. *WIREs Computational Molecular Science* **4**, 15–25 (2013). URL https://onlinelibrary.wiley.com/doi/abs/10.1002/wcms.1159. https://onlinelibrary.wiley.com/doi/pdf/10.1002/wcms.1159.

[8] VandeVondele, J. & Hutter, J. Gaussian basis sets for accurate calculations on molecular systems in gas and condensed phases. *The Journal of Chemical Physics* **127**, 114105 (2007). URL https://doi.org/10.1063/1.2770708. https://doi.org/10.1063/1.2770708.

[9] Krack, M. Pseudopotentials for H to Kr optimized for gradient-corrected exchange-correlation functionals. *Theoretical Chemistry Accounts* **114**, 145 (2005). URL https://doi.org/10.1007/s00214-005-0655-y. https://doi.org/10.1007/s00214-005-0655-y.

[10] Martyna, G. J. & Tuckerman, M. E. A reciprocal space based method for treating long range interactions in ab initio and force-field-based calculations in clusters. *The Journal of Chemical Physics* **110**, 2810–2821 (1999). URL https://doi.org/10.1063/1.477923. https://doi.org/10.1063/1.477923.

[11] Voronina, E. N. *et al.* Mechanisms of hydrogen atom interactions with MoS_2 monolayer. *Journal of Physics: Condensed Matter* **32**, 445003 (2020). URL http://iopscience.iop.org/10.1088/1361-648X/aba013.

[12] Rakhimova, T. V. *et al.* Recombination of o and h atoms on the surface of nanoporous dielectrics. *IEEE Transactions on Plasma Science* **37**, 1697–1704 (2009).

[13] Ziesel, J. P., Schulz, G. J. & Milhaud, J. S formation by dissociative attachment in OCS and CS_2. *The Journal of Chemical Physics* **62**, 1936–1940 (1975). URL https://doi.org/10.1063/1.430681. https://doi.org/10.1063/1.430681.

[14] Stull, D. R. & Prophet, H. *JANAF Thermochemical Tables* (U.S. Dept. of Commerce, National Bureau of Standards, Washington, DC, USA, 1971).